nature chemistry

ARTICLES

https://doi.org/10.1038/s41557-020-00563-4

Check for updates

Frenkel excitons in heat-stressed supramolecular nanocomposites enabled by tunable cage-like scaffolding

Kara Ng[1,2], Megan Webster[3], William P. Carbery[2,4], Nikunjkumar Visaveliya[2], Pooja Gaikwad[1,2], Seogjoo J. Jang[5], Ilona Kretzschmar[1,3] and Dorthe M. Eisele[1,2] ✉

Delocalized Frenkel excitons—coherently shared excitations among chromophores—are responsible for the remarkable efficiency of supramolecular light-harvesting assemblies within photosynthetic organisms. The translation of nature's design principles to applications in optoelectronic devices has been limited by the fragility of the supramolecular structures used and the delicate nature of Frenkel excitons, particularly under mildly changing solvent conditions and elevated temperatures and upon deposition onto solid substrates. Here, we overcome those functionalization barriers through composition of stable supramolecular light-harvesting nanotubes enabled by tunable (~4.3–4.9 nm), uniform (±0.3 nm) cage-like scaffolds. High-resolution cryogenic electron microscopy, combined with scanning electron microscopy, broadband femtosecond transient absorption spectroscopy and near-field scanning optical microscopy revealed that excitons within the cage-like scaffolds are robust, even under extreme heat stress, and control over nanocomposite dimensions is maintained on solid substrates. Our bio-inspired nanocomposites provide a general framework for the development of next-generation organic devices made from stable supramolecular materials.

The future of sustainable energy technologies requires highly efficient and robust light-harvesting materials, especially as rising global temperatures threaten the efficiency of existing photovoltaic installations[1,2]. While breakthroughs in the engineering of large bandgap and multi-excitonic materials may abate temperature-dependent efficiency losses[3–6], it remains unclear how photovoltaic device stability and efficiency will perform under compounding environmental stressors[7–9]. Unlike current solar energy conversion technologies, natural photosynthetic organisms have clearly evolved beyond these challenges, capturing and transporting solar energy at remarkable efficiencies, even under extreme environmental stress[10–12].

Supramolecular assemblies, such as those found in light-harvesting antenna complexes of photosynthetic plants or bacteria[13–15], consist of close-packed molecules self-assembled into ordered structures[15–20]; this close-packing arrangement leads to strong excitation transfer interactions between their molecular transition dipole moments, resulting in new electronic states: Frenkel excitons[21–23]. These new, delocalized excited states—key to the photosynthetic organism's ability to harvest light and transfer excitation energy so efficiently[17,24]—intimately depend on the details of the supramolecular assemblies' molecular packing. Incredibly, despite both the assemblies' structural fragility and their delicate structure–function relationships, some photosynthetic organisms achieve remarkably robust light-harvesting efficiency, even under extreme environmental stress[20,25]. Although the details of photosynthesis may differ considerably within the various natural organisms, their basic design principle remains the same; the light-harvesting antenna's molecular chromophores (that is, supramolecular assemblies) are embedded within a protein or lipid scaffold[26]. This scaffold is thought to be fundamental to both the organism's functionality and robustness[20,27], simultaneously stabilizing the light-harvesting complex's fragile supramolecular structure while enabling it to dynamically respond to external stimuli. As the supramolecular structures of light-harvesting assemblies are held via weak non-covalent interactions, and are thus intrinsically unstable, the stabilizing scaffold is crucial towards preserving the assemblies' intriguing optoelectronic properties (for example, narrow photoemission line shapes[28,29], large Frenkel exciton delocalization and diffusion length[30,31], and high photoconductivity[32]).

Despite tremendous progress towards a deeper understanding of these photosynthetic complexes, as well as progress in the development of organic solar cells[33–35], the possibility of using bio-inspired molecular nanostructures for large-scale solar energy conversion has not yet been realized. Towards efforts to take advantage of nature's successful design pattern for man-made devices, the fundamental question arises: is it possible to design an artificial supramolecular light-harvesting assembly that is: (1) highly stable (that is, stabilize its fragile structure against disassembly or reassembly processes under de-stabilizing solvent conditions); (2) robust (that is, maintain its Frenkel excitonic character against extreme and fluctuating environments); and (3) viable for device integration (that is, capable of being immobilized onto solid substrate)? If so, bio-inspired supramolecular assemblies may finally serve as a usable light-harvesting material system for the development of future solar energy conversion technologies based on stable supramolecular materials.

Here, we address this fundamental question via a chemical, solution-based route—in situ template-directed self-assembly—to

[1]PhD Program in Chemistry, Graduate Center, The City University of New York, New York, NY, USA. [2]Department of Chemistry and Biochemistry, The City College of New York at The City University of New York, New York, NY, USA. [3]Department of Chemical Engineering, The City College of New York at The City University of New York, New York, NY, USA. [4]Department of Chemistry, New York University, New York, NY, USA. [5]Department of Chemistry and Biochemistry, Queens College at The City University of New York, New York, NY, USA. ✉e-mail: Eisele@eiselegroup.com

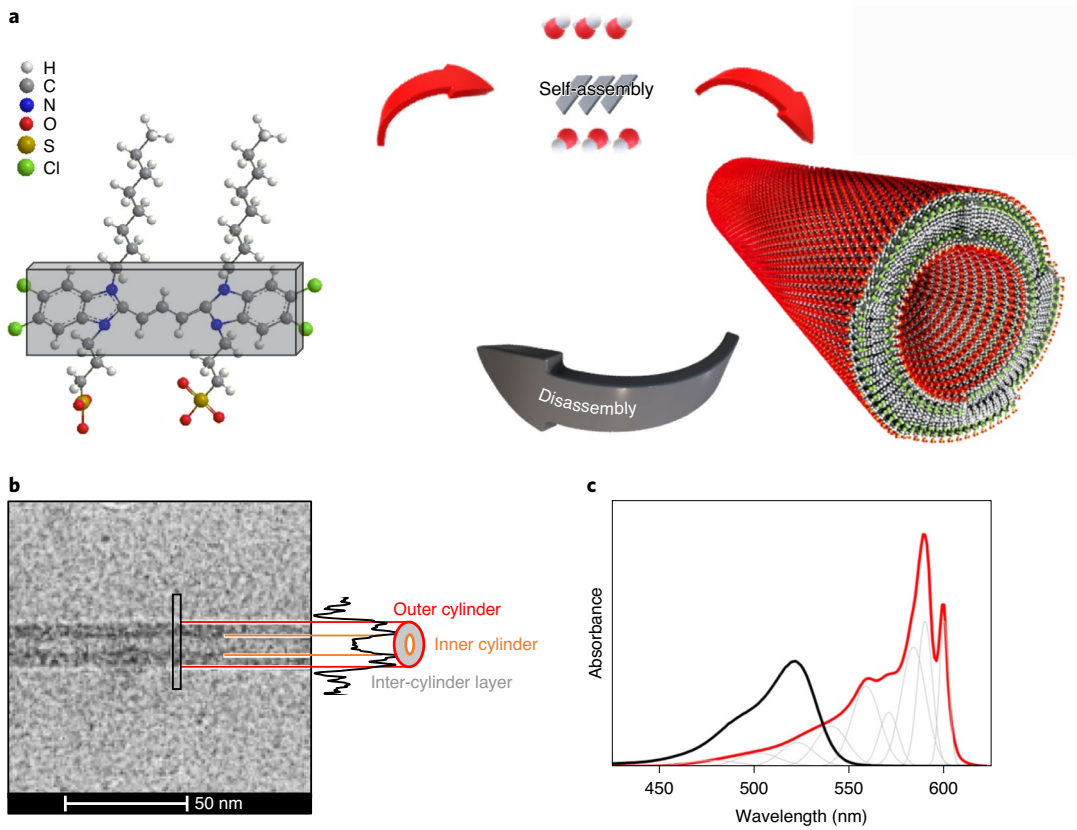

Fig. 1 | Supramolecular LHNTs assembled from the cyanine dye derivative C8S3. a, Schematic of amphiphilic cyanine dye (C8S3) monomers (chromophore shown in grey) self-assembling in aqueous solution (see Methods) into metastable assemblies of bi-layered supramolecular LHNTs. In general, supramolecular assemblies, including these LHNTs, are self-assembled via weak, non-covalent interactions; thus, they are subject to spontaneous disassembly into free (non-assembled) monomers. **b**, High-resolution cryo-TEM micrograph of an individual LHNT, with the contrast pattern from a line scan taken perpendicularly across the LHNT (black), indicates areas of increased electron density and confirming the bi-layered structure. **c**, Ultraviolet–visible absorption spectrum of monomers (black) and supramolecular LHNTs (red). Upon self-assembly into LHNTs, strong excitation transfer interactions lead to red-shifted and narrowed Frenkel exciton transitions; the overall shape of the absorption spectrum can be fitted by convolution of at least eight overlapping Frenkel exciton transitions (grey). The main exciton transition 1 (smaller narrow red peak at ~600 nm in **c**) and transition 2 (larger narrow red peak at ~590 nm in **c**), which correspond to the inner (orange in **b**) and outer cylinders (red in **b**) respectively, are well separated and clearly resolved from one another. Schematic of LHNT in panel **a** adapted with permission from ref. [36], Springer Nature Ltd.

design well-defined bio-inspired supramolecular light-harvesting nanocomposites that are highly stable, robust and device ready. First, to mimic the Frenkel excitonic properties of the natural light-harvesting antennae complex, we utilized well-defined, well-characterized supramolecular light-harvesting nanotubes (LHNTs)[36–38] self-assembled from synthetic molecular chromophores in aqueous solution. Specifically, we used amphiphilic cyanine dye, 3,3′-bis(2-sulphopropyl)-5,5′,6,6′-tetrachloro-1,1′-dioctylbenz-imideacarbocyanine (C8S3; Fig. 1a) that self-assembles in aqueous solution into highly uniform bi-layered supramolecular nanotubes comprised of an inner cylinder and an outer cylinder (Fig. 1b). Upon self-assembly into LHNTs, the characteristically broad absorption spectrum of the monomers undergoes a large red-shift and line narrowing (Fig. 1c), indicative of exceptionally strong excitation transfer interactions between the close-packed molecules and large Frenkel exciton delocalization. Second, to develop a stabilizing scaffold, we propose an in situ encapsulation strategy: cage-like scaffolding. Unlike previous encapsulation strategies, which utilize high-density, high-molecular-weight polymers to solidify the ensemble into a thin film[39] or sugar matrix[40], we propose utilizing small, non-excitonic silane molecules that are capable of self-assembly in aqueous solution to form a cage-like scaffold to stabilize the entire supramolecular structure of LHNTs.

While solid-state encapsulation strategies are staple for device processing of non-assembled molecules and inorganic nanostructures, they neglect the fragility of supramolecular assemblies' internal structures. The internal order of the molecules within the assemblies is intrinsically unstable—readily disassembling, reassembling or degrading, even under mildly changing environmental conditions—as the molecular subunits in supramolecular assemblies are held together exclusively by weak, non-covalent interactions[41]. Furthermore, the high-molecular-weight polymers used for encapsulation are typically too large to infiltrate the intermolecular space between closely packed chromophores; thus, these encapsulation strategies would only achieve an outer, protective shield on the surface of the assemblies. The highly delicate structure–function relationship of the assemblies compounds the problem of their structural instability; the internal structure of supramolecular assemblies is easily distorted by stabilization methods involving high-molecular-weight polymers, thus easily destroying the delicate Frenkel excitonic character of the materials. It is also unclear how and to what extent these stabilization methods contribute to disorder effects of the supramolecular system, which also heavily influence the resulting optoelectronic properties[42]. Even at lower concentrations of polymers, at which the assemblies do not undergo catastrophic structural collapse, the internal order (which is respon-

sible for the strong excitation transfer interactions between their molecular transition dipole moments) may not be maintained. In fact, we found that even the addition of low-molecular-weight polyelectrolytes (a more recent method employed to stabilize supramolecular assemblies[43,44]) was not successful in preventing structural reassembly of the LHNTs (Supplementary Section 1). For these LHNTs and other supramolecular assemblies, solid-state and polymer encapsulation are not viable strategies for the development of stable supramolecular assemblies.

In contrast, scaffolds self-assembled from small molecules may overcome these challenges. We propose that, if they can slip in between the closely packed (~5 Å) chromophores of the supramolecular assemblies, small molecules can be utilized to form a cage-like scaffold that stabilizes not only the surface of the assembly but also permeates the supramolecular structure to stabilize the assemblies' internal structure against disassembly and reassembly processes, even under extreme environmental stress.

Results and discussion

Synthesis of the cage-like scaffold. We assembled our proposed cage-like scaffold by encapsulating LHNTs with cross-linking molecular silanes: (3-aminopropyl)trimethoxysilane (APTMS) and tetraethyl orthosilicate (TEOS). Cryogenic transmission electron microscopy (cryo-TEM) micrographs taken from shock-frozen solution revealed that the scaffold was incredibly uniform along an individual LH nanotube (±0.1 nm), as well as between different LH nanotubes within an ensemble (±0.3 nm) (Fig. 2a,b), potentially due to the kinetic mismatch in the hydrolysis–condensation process between methoxy- and ethoxy-substituted silanes leading to more controlled condensation along the surfaces of LHNTs (Supplementary Section 2). The two-step scaffold assembly was first mediated by the electrostatic binding between the protonated amino silane and negatively charged sulfonate surface of the LHNTs, and then proceeded through the condensation of hydrolysed silanol to form a highly cross-linked SiO_2 network (Supplementary Fig. 4). Because our scaffolding SiO_2 network should be less flexible than conventional polymers used in previous stabilization attempts (and thus not as amenable to swelling and shrinking processes that may lead to supramolecular re-arrangements), our proposed in situ scaffolding may serve as a general framework for processing supramolecular assemblies for future device integration. Compared with unscaffolded LHNTs, which exhibit a distinct high-/low-contrast pattern associated with the relatively electron-deficient alkyl side chains that make up the inter-cylinder layer between the electron-rich outer and inner cylinders, cryo-TEM analysis of our scaffolded LHNTs revealed that the low-contrast pattern associated with the inter-cylinder layer was replaced with an additional high-contrast pattern (that is, increased electron density along the inter-cylinder layer) (Fig. 2b). The increase in electron density along the inter-cylinder layer can be rationalized by, for example, infiltration of silica along the supramolecular structure (cage-like scaffolding) or distortion of the supramolecular assemblies' internal structures upon scaffolding. To determine whether the scaffold network preserved the LHNTs' supramolecular structures, we assessed the scaffolds' architecture by monitoring the LHNTs' well-defined structure-dependent optical properties.

Maintaining the supramolecular structure of LHNTs upon scaffolding. To assess whether the scaffold distorted or destroyed the supramolecular structure of the LHNTs, we monitored changes to the absorption spectra of the LHNTs before and after scaffolding via ultraviolet–visible absorption spectroscopy, as a plethora of information about assemblies' structure-dependent Frenkel excitonic properties is indirectly implied in the absorption spectrum[45] (for example, electronic coupling strength, delocalization length, exciton mobility and diffusion, and inelastic exciton–exciton interactions). Remarkably, the absorption and emission spectra of LHNTs before and after scaffolding were nearly indistinguishable (Fig. 2c); the emission line width of the inner-cylinder transition was virtually unchanged upon scaffolding (from 153 ± 5 to 150 ± 5 cm^{-1}), indicating that the Frenkel excitonic character was well maintained and that the use of molecular silanes is uniquely effective for assembling well-defined scaffolds without altering the delicate supramolecular structure of LHNTs.

These results were further supported by ultrafast spectroscopy; as the optical properties of supramolecular assemblies are determined by the ultrafast formation and transport of delocalized excitons[46], we utilized broadband femtosecond transient absorption spectroscopy to compare the exciton lifetime in LHNTs before and after scaffolding. Singular value decomposition of transient absorption spectra was performed to yield decay-associated difference spectra. The fitting of transient absorption spectra returned short (τ_1) and long (τ_2) lifetime components of 7.7 ± 0.4 ps and 850.3 ± 43.4 ps for unscaffolded LHNTs and 7.3 ± 0.9 ps and 928 ± 177.4 ps for scaffolded LHNTs, respectively (Supplementary Fig. 6). Despite the wider confidence interval in the scaffolded LHNTs sample due to relatively low overall signal in the transient absorption, both short- and long-lifetime components in the unscaffolded LHNTs and scaffolded LHNTs were comparable. These results further support that the electrostatic-mediated binding between protonated amino-functionalized silane and the LHNTs' negatively charged sulfonate surfaces did not substantially alter the LHNTs' structure-dependent exciton dynamics. As the self-assembly of the scaffold did not affect the supramolecular structure and Frenkel excitonic properties of the LHNTs, we utilized the structural assignments of spectroscopic features previously established for LHNTs and applied these same assignments to the scaffolded LHNTs.

Scaffolded LHNTs are structurally stable under environmental stress. We monitored the main excitonic transitions 1 and 2, which are attributed to the inner and outer cylinders respectively, under structurally de-stabilizing solvent conditions, providing evidence that our scaffold stabilizes the weakly bound supramolecular structure against disassembly and reassembly processes. In Fig. 2d (red), the extent of the unscaffolded LHNTs' intrinsic structural instability is immediately evident, with excitonic transition 2 rapidly decreasing upon the introduction of slight changes to the solvent as the outer cylinder experiences a higher degree of exposure to the surrounding environment. Most notably, increasing the methanol concentration of the LHNTs solution resulted in a rapid increase in non-assembled monomer transitions at ~520 nm as the Frenkel exciton transitions at ~550–600 nm decreased (Supplementary Fig. 7). Decreasing the dye concentration under constant solvent polarity caused similar trends (Fig. 2d, red). The destruction of LHNTs and their corresponding disassembly to non-assembled monomers under mild changes to solvent conditions can be rationalized by considering the initial driving forces of self-assembly. Because the amphiphilic cyanine monomers are driven into bi-layers by hydrophobic forces and subsequently coupled through π–π stacking interactions, we expect to drive a disassembly process by decreasing the solvent polarity or decreasing the dye concentration. It is clear from the loss of both excitonic transitions 1 and 2 in unscaffolded LHNTs that both inner and outer cylinders become structurally unstable.

In stark contrast with unscaffolded LHNTs, scaffolded LHNTs demonstrated remarkable retention of both excitonic transitions 1 and 2 in solutions with in excess of 26% methanol by volume (Supplementary Fig. 7) and at dye concentrations well under the critical aggregation concentration (Fig. 2d, blue), as well as in highly acidic and basic solutions, indicating that the supramolecular structure of scaffolded LHNTs was stabilized against disassembly to non-assembled monomers (Supplementary Fig. 8). A minor increase in non-assembled monomer transition upon decreasing

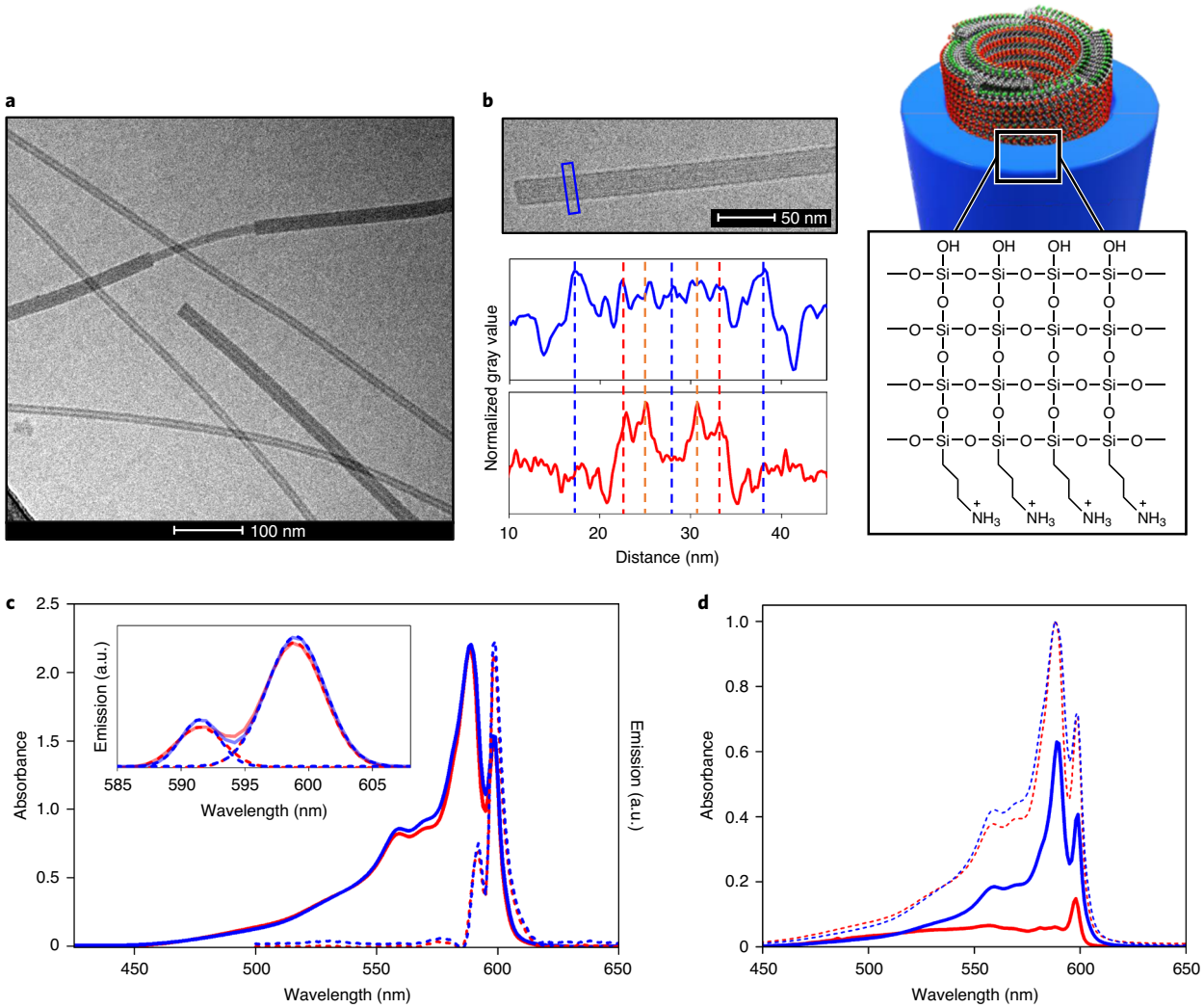

Fig. 2 | Stable supramolecular nanocomposites via cage-like scaffold design. a, Representative cryo-TEM micrograph of a shock-frozen solution supramolecular nanocomposite sample, revealing the presence of both scaffolded and unscaffolded LHNTs in the ensemble. The observed scaffolded LHNTs were highly uniform, both along individual LHNTs (±0.1 nm) and between different LHNTs (±0.3 nm). **b**, Top left: high-resolution cryo-TEM micrograph of a scaffolded LHNT observed in a shock-frozen supramolecular nanocomposite sample of a 3:1:1 molar ratio of C8S3:APTMS:TEOS. Bottom left: the contrast pattern of the line scan profile of scaffolded LHNT (blue; taken from the region indicated in the image above) is overlaid with that of an unscaffolded supramolecular LHNT (red; taken from Fig. 1b), supporting the possibility of cage-like scaffolding (that is, infiltration of silica within the inter-cylinder layer and along the inner cylinder, as well as the scaffolding of the outer cylinder). The dimensions of the scaffolded LHNTs were 22.4 ± 0.2 nm. The scaffold dimensions were 4.9 ± 0.1 nm. The schematic (right) depicts the morphology of scaffolded LHNT and the molecular structure of the silica scaffold. **c**, Ultraviolet–visible absorption (solid) and emission (dotted) spectra of LHNTs before (red) and after scaffolding (blue). Inset: emission spectra were fitted assuming two Gaussian excitonic transitions for outer- and inner-cylinder transitions (dotted). No significant broadening of the line width was observed upon scaffolding, indicating no substantial changes to exciton delocalization upon scaffolding. **d**, De-stabilizing solvent conditions (for example, dilution below the critical aggregation concentration, from 0.39 mM (dotted) to 0.12 mM (solid)) were introduced to assess the structural stability of supramolecular LHNTs before (red) and after scaffolding (blue). Under structurally de-stabilizing solvent conditions, substantial loss of excitonic character and disassembly into free (non-assembled) monomers was observed for unscaffolded LHNTs (red) while scaffolded LHNTs (blue) retained the excitonic character of outer- and inner-cylinder transitions. Schematic of LHNT in panel **b** adapted with permission from ref. [37], Springer Nature Ltd.

the solvent polarity was consistent with observations of partially or non-scaffolded LHNTs in the cryo-TEM of scaffolded LHNT solution (Fig. 2a), as we expect the non-scaffolded LHNTs in solution to disassemble into free (non-assembled) monomers under these conditions. Critically, we demonstrated that both the inner and outer cylinders were structurally intact in the scaffolded LHNTs, suggesting that the scaffolding SiO_2 network may provide more than a protective outer layer, forming in addition an interlocking cross-linked network between the closely packed molecules to prevent their disassembly. The remarkable structural stability, combined with the improved chemical stability under acidic and basic pH and the slightly improved photostability under high-intensity illumination (Supplementary Fig. 9), are all highly indicative that scaffolded LHNTs can be a breakthrough light-harvesting material system for future photovoltaic applications.

Scaffolded LHNTs are robust against extreme heat stress. The next critical consideration in efforts to adopt supramolecular assemblies for future solar energy conversion applications is the stability of supramolecular assemblies under environmental

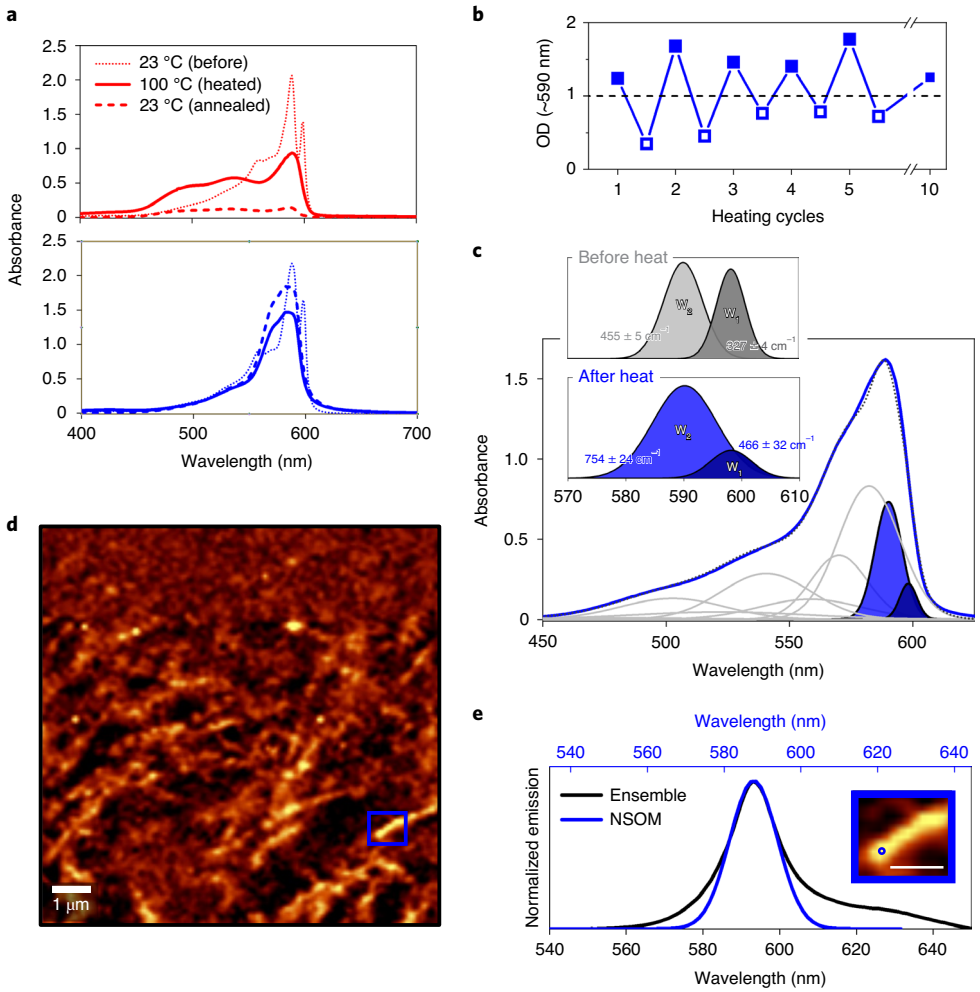

Fig. 3 | Robust Frenkel excitons in supramolecular nanocomposites despite extreme heat stress. a, Ultraviolet–visible absorption spectra of supramolecular LHNTs (top; red) and scaffolded LHNTs (bottom; blue). The LHNT solution after heating to 100 °C (solid; red) indicated destruction of the supramolecular structure (that is, significant loss of the excitonic character simultaneously with an increase in the free (non-assembled) monomer spectral signature) and thermal degradation (as evidenced by continued loss of optical density even after annealing to 23 °C (dashed; red)). In contrast, upon heating of the scaffolded LHNTs, excitonic transitions were maintained without an increase in the free (non-assembled) monomer signature (solid; blue); thus, the excitonic character was maintained with no structural disassembly (Supplementary Section 5). Rather than continued degradation, the optical density of the excitonic transition recovered upon annealing (dashed; blue). **b**, Repeated heat stress (multiple cycles of heating and annealing) of scaffolded LHNTs demonstrated that optical self-healing is reproducible over at least ten cycles, indicating that Frenkel excitons in scaffolded LHNTs are robust against extreme and fluctuating temperature conditions. OD, optical density. **c**, Spectral decomposition of scaffolded LHNTs after heat stress. The shape of the experimental scaffolded LHNT spectrum (blue) was reproduced (dotted; black) assuming nine convolved excitonic transitions (see Fig. 1c). Inset: line widths (W) before (grey) and after heat stress (blue) obtained from fitting excitonic transitions 1 and 2 to Gaussian functions. Changes to the energetic peak separation and broadening of the combined line widths of excitonic transitions 1 and 2 were observed upon heat stress. Because these changes were small (~100–300 cm^{-1}) relative to intermolecular coupling (1,500 cm^{-1}), they were not expected to significantly affect exciton mobilities. **d**, Spectrally resolved fluorescence NSOM (Supplementary Fig. 16) emission image of scaffolded LHNTs after exposure to extreme heat stress. Emission spectra were collected during a raster scan over 150 × 150 individual points along a 10 μm × 10 μm image. The sum-filter of the emission maximum (λ_{em} = 590 nm) was applied over 22,500 spectra to produce the NSOM emission image. Emissive quasi-1D nanostructures were observed in NSOM emission, consistent with nanostructures observed in SEM micrographs of heat-stressed scaffolded LHNTs (Supplementary Fig. 13). **e**, Double *xy* plot comparing the fitted near-field and ensemble emissions of scaffolded LHNTs after repeated heat stress. The near-field emission collected from the sub-diffraction spot (Supplementary Fig. 14) and fitted to the Gaussian function was consistent with the ensemble fluorescence line shape, with a minor blue shift consistent with solvent effects (that is, drying). Inset: magnification of the emissive quasi-1D nanostructure observed in NSOM emission (**d**), to illustrate the optical spatial resolution of imaging (~60 nm), which is limited by aperture dimensions and pixel binning. Scale bar, 500 nm.

stress, such as extreme temperature fluctuations. Typically, supramolecular assemblies are highly unstable at elevated temperatures because excess vibrational energy will distort the optimal packing geometry, consequently destroying the assemblies' Frenkel excitonic character. In Fig. 3, we demonstrate how solution-based in situ scaffolding of LHNTs can overcome this intrinsic thermal instability. For unscaffolded LHNTs, as expected, a substantial increase in the spectral signature of non-assembled monomers and a substantial decrease in exciton transitions was observed upon a temperature increase to 100 °C (heating), and both changes were associated with destruction of the structure of the LHNTs, followed by a complete loss of optical density upon letting the solution return to room

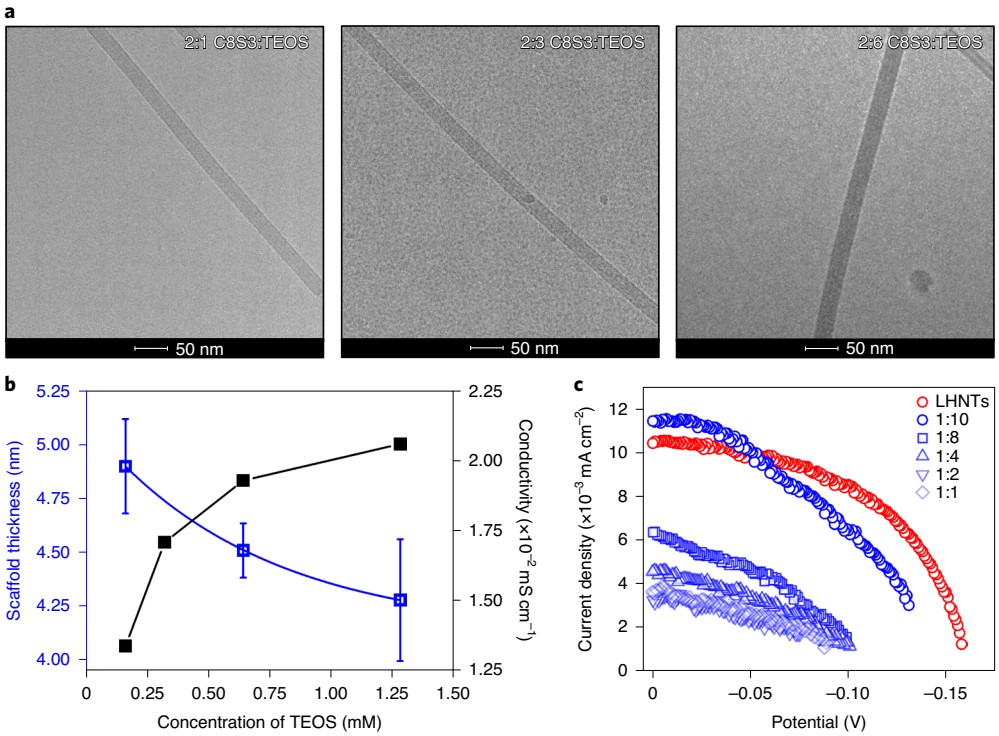

Fig. 4 | Discrete tunability of supramolecular nanocomposites' scaffold dimensions in solution and on substrate. a, Representative cryo-TEM micrographs of scaffolded LHNTs prepared with increasing molar ratios of TEOS reveal homogeneous scaffolding. **b**, Mean and standard deviation of scaffold dimensions (blue) with increasing TEOS concentration. The scaffold dimensions obtained from cryo-TEM were consistent with discrete monolayer tunability with increasing TEOS concentration. Larger scaffold dimensions were consistent with decreasing conductivity (black), as increasing distance between the negatively charged LHNT surface and positive counter-ions would result in decay of the surface conductivity. **c**, Current density–voltage curves of supramolecular LHNTs (red) and scaffolded LHNTs (blue). The PCE of cells sensitized with scaffolded LHNTs decreased rapidly with increasing scaffold dimensions (the legend shows the monomer ratio C8S3:TEOS), suggesting that the scaffold tunability observed in solution was retained when isolated from solution and immobilized onto solid substrate.

temperature (annealing) (Fig. 3a, red), which was associated with thermal degradation of the material. In contrast, upon heating and annealing (herein, referred to as heat stress) of the scaffolded LHNTs in solution, neither the spectral signature of disassembly nor thermal degradation was observed (Fig. 3a, blue). Most interestingly, the overall changes in the shape of scaffolded LHNTs' absorption and emission spectra indicated that Frenkel excitonic features (that is, the large spectral red-shift relative to monomer transition and line narrowing of exciton transitions) were maintained upon heat stress (Supplementary Fig. 10). In addition, the loss of excitonic oscillator strength observed at high temperatures was reversible in scaffolded LHNTs over several heat stress cycles (Fig. 3b), demonstrating that scaffolded LHNTs are not only remarkably robust against heat stress, but are also robust against exposure to extreme thermal fluctuations.

While the structural origin of the heat-stress-induced changes to the scaffolded LHNT spectra is non-trivial to elucidate, analysis of the individual excitonic transitions convolved within the congested absorption spectrum can discern whether the observed spectral changes are expected to substantially affect the excitonic properties of the LHNTs (Supplementary Section 5). The absorption spectra of scaffolded LHNTs before and after heat stress were fit with nine Gaussian functions associated with the eight previously attributed excitonic transitions of LHNTs and the transitions of the free (non-assembled) monomer (Fig. 3c). Upon heat stress, a slight increase in line width was observed for excitonic transitions 1 and 2: approximately 150 and 300 cm^{-1}, respectively (Fig. 3c, inset). The spectral broadening of excitonic transitions, as well as the slight decrease in the energetic positions between exciton transitions 1 and 2 (Supplementary Figs. 11 and 12), suggest that the changes to the overall shape of the absorption spectra upon heat stress reflect local changes in the scaffolded LHNTs' environment as well as thermal broadening due to excitation of vibrational modes, such that the inner and outer cylinders are more similar (that is, their spectral features are no longer clearly resolved in the spectrum). All of the observed changes in the spectra are small compared with the resonance interactions between nearest-neighbour molecules (~1,500 cm^{-1}); thus, they are not expected to affect exciton delocalization and mobilities substantially.

Although the supramolecular structure of scaffolded LHNTs upon heat stress cannot be directly imaged by even the highest-resolution microscopy techniques, we used a combination of scanning electron microscopy (SEM; Supplementary Fig. 13) and fluorescence near-field scanning optical microscopy (NSOM; Fig. 3d) to correlate the assemblies' morphology and optical properties. Both SEM and NSOM revealed that the assemblies' morphology was consistent with quasi-one-dimensional (quasi-1D) nanostructures (Fig. 3e, inset). Near-field emission collected from sub-diffraction (~60 nm) segments along the LHNT was fit to a Gaussian function and compared with that of far-field ensemble emission (Fig. 3e). The near-field and far-field emission spectra were remarkably similar, with no substantial line broadening, but a minor energy shift in the emission spectrum was observed (Supplementary Fig. 14). The observation of emissive quasi-1D nanostructures in NSOM provided strong evidence that scaffolded LHNTs are robust against heat stress, as we would expect the weakly bound supramolecular structures to be destroyed under extreme temperatures (Fig. 3a). Additionally, the observed changes to the excitonic transitions

occurred without a corresponding increase in free (non-assembled) monomers, ruling out structural disassembly and reassembly processes. Together, these results suggest that the proposed scaffold probably adopts an interlocking formation throughout the supramolecular structure, which substantially stabilizes the weakly held assemblies against disassembly. The superior thermal stability of scaffolded LHNTs was also observed not only in solution but also upon immobilization onto solid substrate (Supplementary Fig. 15). The robustness of the Frenkel excitons under extreme heat stress makes scaffolded LHNTs a highly promising material to bring supramolecular assemblies for solar energy harvesting from fundamental research to real world applications.

Scaffold tunability. Finally, maintaining precise control over the scaffolds' dimensions—key for designing and manipulating interfacial transport properties—while immobilizing them onto solid substrates will be crucial towards utilizing scaffolded supramolecular assemblies for further fundamental investigations as well as in practical device applications. Based on analysis of numerous cryo-TEM micrographs under varying TEOS concentrations (Fig. 4a), we found that the scaffold thickness was discretely tunable between ~4.3–4.9 nm, and sub-nanometre control of the scaffold thickness was consistent with discrete monolayer tunability (Fig. 4b, blue). Surface conductivity measurements in solution revealed that the double-layer electrical conductivity of scaffolded LHNTs decayed with increasing scaffold diameter, consistent with a decay of excess conductivity at the system's diffuse layer with each monolayer addition of SiO_2 (Fig. 4b, black). Complementary substrate studies were performed to independently verify that the scaffolded LHNTs retained thickness control of the scaffold when isolated out of solution and immobilized onto solid substrate. As an example, we tested the power conversion efficiency (PCE) of scaffolded LHNTs as sensitizers in an adhesive-sealed dye-sensitized solar cell (DSSC) device. As the sub-nanometre interfacial distance between the working electrode and sensitizer increased, the percentage PCE decreased rapidly, confirming that precise scaffold tunability was retained when the scaffold was immobilized from solution onto a substrate (Fig. 4c). The discrete monolayer tunability in solution and on substrate provides evidence that the presented scaffolded LHNTs are viable for device integration and hold the potential to serve as an excellent, well-defined model system in future work to directly probe sensitive distance-dependent exciton, plexciton and charge-transfer dynamics in hybrid systems.

Summary. Successful integration of supramolecular assemblies into large-scale optoelectronic device applications has not been realized yet, mainly due to their intrinsic structural instability, resulting in strong degradation under even mild solvent and temperature changes. Our experiments provide a proof-of-concept demonstration that these intrinsic barriers towards the functionalization of artificial supramolecular assemblies can be largely overcome through cage-like scaffolding of the individual assembly in solution. Our chemical, solution-based route for in situ template-directed self-assembly is a successful scaffolding strategy for the design of bio-inspired supramolecular light-harvesting nanocomposites with a surprisingly stable (that is, stable against disassembly, even under extreme environmental changes) and highly robust supramolecular structure (that is, maintaining Frenkel excitonic character even under extreme heat stress). The unprecedented scaffold tunability of our light-harvesting nanocomposites allows for future functionalization with diverse material systems to engineer unique optoelectronic properties. In addition, discrete monolayer tunability in solution was maintained upon immobilization onto a solid substrate, enabling supramolecular nanostructures such as LHNTs to finally be used for future integration into solid-state devices. Our findings hold the potential for an immediate impact on critical yet unresolved research questions (for example, the fundamental role of the protein environment on photosynthetic light harvesting and controlling nanoscale and interfacial transport). Moreover, our nanocomposite light-harvesting model system will enable investigations that were previously not possible (for example, the dilution of supramolecular assemblies required for single-molecule imaging or precise tunability of scaffold dimensions in situ for controlled functionalization of hybrid model systems).

Online content

Any methods, additional references, Nature Research reporting summaries, source data, extended data, supplementary information, acknowledgements, peer review information; details of author contributions and competing interests; and statements of data and code availability are available at https://doi.org/10.1038/s41557-020-00563-4.

Received: 9 September 2019; Accepted: 16 September 2020;
Published online: 16 November 2020

References

1. Sheikh, A. D. et al. Effects of high temperature and thermal cycling on the performance of perovskite solar cells: acceleration of charge recombination and deterioration of charge extraction. *ACS Appl. Mater. Interfaces* **9**, 35018–35029 (2017).
2. Peters, I. M. & Buonassisi, T. The impact of global warming on silicon PV energy yield in 2100. Preprint at https://arxiv.org/abs/1908.00622 (2019).
3. Dash, P. K. & Gupta, N. C. Effect of temperature on power output from different commercially available photovoltaic modules. *J. Eng. Res. Appl.* **5**, 148–151 (2015).
4. Weiss, L. R. et al. Strongly exchange-coupled triplet pairs in an organic semiconductor. *Nat. Phys.* **13**, 176–181 (2017).
5. Pun, A. B. et al. Ultra-fast intramolecular singlet fission to persistent multiexcitons by molecular design. *Nat. Chem.* **11**, 821–828 (2019).
6. Einzinger, M. et al. Sensitization of silicon by singlet exciton fission in tetracene. *Nature* **571**, 90–94 (2019).
7. Tai, Q. et al. Efficient and stable perovskite solar cells prepared in ambient air irrespective of the humidity. *Nat. Commun.* **7**, 11105 (2016).
8. Tan, H. et al. Efficient and stable solution-processed planar perovskite solar cells via contact passivation. *Science* **355**, 722–726 (2017).
9. Xu, X. et al. Thermally stable, highly efficient, ultraflexible organic photovoltaics. *Proc. Natl Acad. Sci. USA* **115**, 4589–4594 (2018).
10. Beatty, J. T. et al. An obligately photosynthetic bacterial anaerobe from a deep-sea hydrothermal vent. *Proc. Natl Acad. Sci. USA* **102**, 9306–9310 (2005).
11. Tang, K.-H. et al. Temperature and ionic strength effects on the chlorosome light-harvesting antenna complex. *Langmuir* **27**, 4816–4828 (2011).
12. Maiuri, M., Ostroumov, E. E., Saer, R. G., Blankenship, R. E. & Scholes, G. D. Coherent wavepackets in the Fenna–Matthews–Olson complex are robust to excitonic-structure perturbations caused by mutagenesis. *Nat. Chem.* **10**, 177–183 (2018).
13. Rolczynski, B. S. et al. Correlated protein environments drive quantum coherence lifetimes in photosynthetic pigment–protein complexes. *Chem* **4**, 20–21 (2018).
14. Blau, S. M., Bennett, D. I. G., Kreisbeck, C., Scholes, G. D. & Aspuru-Guzik, A. Local protein solvation drives direct down-conversion in phycobiliprotein PC645 via incoherent vibronic transport. *Proc. Natl Acad. Sci. USA* **115**, E3342–E3350 (2018).
15. Romero, E. et al. Quantum coherence in photosynthesis for efficient solar-energy conversion. *Nat. Phys.* **10**, 676–682 (2014).
16. Collini, E. et al. Coherently wired light-harvesting in photosynthetic marine algae at ambient temperature. *Nature* **463**, 644–647 (2010).
17. Ishizaki, A., Calhoun, T. R., Schlau-Cohen, G. S. & Fleming, G. R. Quantum coherence and its interplay with protein environments in photosynthetic electronic energy transfer. *Phys. Chem. Chem. Phys.* **12**, 7319–7337 (2010).
18. Scholes, G. D., Fleming, G. R., Olaya-Castro, A. & van Grondelle, R. Lessons from nature about solar light harvesting. *Nat. Chem.* **3**, 763–774 (2011).
19. Jordan, P. et al. Three-dimensional structure of cyanobacterial photosystem I at 2.5 Å resolution. *Nature* **411**, 909–917 (2001).
20. Peers, G. et al. An ancient light-harvesting protein is critical for the regulation of algal photosynthesis. *Nature* **462**, 518–521 (2009).
21. Kasha, M., Rawls, H. R. & Ashraf El-Bayoumi, M. The exciton model in molecular spectroscopy. *Pure Appl. Chem.* **11**, 371–392 (1965).
22. Hestand, N. J. & Spano, F. C. Expanded theory of H- and J-molecular aggregates: the effects of vibronic coupling and intermolecular charge transfer. *Chem. Rev.* **118**, 7069–7163 (2018).

23. Jang, S. J. & Mennucci, B. Delocalized excitons in natural light-harvesting complexes. *Rev. Mod. Phys.* **90**, 035003 (2018).
24. Engel, G. S. et al. Evidence for wavelike energy transfer through quantum coherence in photosynthetic systems. *Nature* **446**, 782–786 (2007).
25. Chmeliov, J. et al. The nature of self-regulation in photosynthetic light-harvesting antenna. *Nat. Plants* **2**, 16045 (2016).
26. Dostál, J., Pšenčík, J. & Zigmantas, D. In situ mapping of the energy flow through the entire photosynthetic apparatus. *Nat. Chem.* **8**, 705–710 (2016).
27. Grewe, S. et al. Light-harvesting complex protein LHCBM9 is critical for photosystem II activity and hydrogen production in *Chlamydomonas reinhardtii*. *Plant Cell* **26**, 1598–1611 (2014).
28. Park, H. et al. Enhanced energy transport in genetically engineered excitonic networks. *Nat. Mater.* **15**, 211–217 (2015).
29. Brixner, T., Hildner, R., Köhler, J., Lambert, C. & Würthner, F. Exciton transport in molecular aggregates—from natural antennas to synthetic chromophore systems. *Adv. Energy Mater.* **7**, 1700236 (2017).
30. Akselrod, G. M. et al. Visualization of exciton transport in ordered and disordered molecular solids. *Nat. Commun.* **5**, 3646 (2014).
31. Haedler, A. T. et al. Long-range energy transport in single supramolecular nanofibres at room temperature. *Nature* **523**, 196–199 (2015).
32. Yamamoto, Y. et al. Photoconductive coaxial nanotubes of molecularly connected electron donor and acceptor layers. *Science* **314**, 1761–1764 (2006).
33. Morseth, Z. A. et al. Interfacial dynamics within an organic chromophore-based water oxidation molecular assembly. *ACS Appl. Mater. Interfaces* **9**, 16651–16659 (2017).
34. Zhang, Q. et al. Highly efficient resonant coupling of optical excitations in hybrid organic/inorganic semiconductor nanostructures. *Nat. Nanotechnol.* **2**, 555–559 (2007).
35. Pace, N. A., Reid, O. G. & Rumbles, G. Delocalization drives free charge generation in conjugated polymer films. *ACS Energy Lett.* **3**, 735–741 (2018).
36. Eisele, D. M., Knoester, J., Kirstein, S., Rabe, J. P. & Vanden Bout, D. A. Uniform exciton fluorescence from individual molecular nanotubes immobilized on solid substrates. *Nat. Nanotechnol.* **4**, 658–663 (2009).
37. Eisele, D. M. et al. Utilizing redox-chemistry to elucidate the nature of exciton transitions in supramolecular dye nanotubes. *Nat. Chem.* **4**, 655–662 (2012).
38. Eisele, D. M. et al. Robust excitons inhabit soft supramolecular nanotubes. *Proc. Natl Acad. Sci. USA* **111**, E3367–E3375 (2014).
39. Higgins, D. A. & Barbara, P. F. Excitonic transitions in J-aggregates probed by near-field scanning optical microscopy. *J. Phys. Chem.* **99**, 3–7 (1995).
40. Caram, J. R. et al. Room-temperature micron-scale exciton migration in a stabilized emissive molecular aggregate. *Nano Lett.* **16**, 6808–6815 (2016).
41. Cleary, L., Chen, H., Chuang, C., Silbey, R. J. & Cao, J. Optimal fold symmetry of LH2 rings on a photosynthetic membrane. *Proc. Natl Acad. Sci. USA* **110**, 8537–8542 (2013).
42. Jang, S. & Cheng, Y. C. Resonance energy flow dynamics of coherently delocalized excitons in biological and macromolecular systems: recent theoretical advances and open issues. *Wiley Interdiscip. Rev. Comput. Mol. Sci.* **3**, 84–104 (2013).
43. Qiao, Y. et al. Nanotubular J-aggregates and quantum dots coupled for efficient resonance excitation energy transfer. *ACS Nano* **9**, 1552–1560 (2015).
44. Al-Khatib, O. et al. Adsorption of polyelectrolytes onto the oppositely charged surface of tubular J-aggregates of a cyanine dye. *Colloid. Polym. Sci.* **297**, 729–739 (2019).
45. Knoester, J. Modeling the optical properties of excitons in linear and tubular J-aggregates. *Int. J. Photoenergy* **2006**, 1–10 (2006).
46. Novoderezhkin, V., Monshouwer, R. & van Grondelle, R. Exciton (de) localization in the LH2 antenna of *Rhodobacter sphaeroides* as revealed by relative difference absorption measurements of the LH2 antenna and the B820 subunit. *J. Phys. Chem. B* **103**, 10540–10548 (1999).

Methods

Preparation of LHNTs. Cyanine dye derivative C8S3 (molecular weight = 902.8 g mol^{-1}; FEW Chemicals) was used as received. Details of the preparation of the LHNTs are described elsewhere[47]. The encapsulation strategy was inspired by previous work[48]. The silanes APTMS (molecular weight = 179.3 g mol^{-1}; Fisher Scientific) and TEOS (molecular weight = 208.3 g mol^{-1}; Fisher Scientific) were stored under argon in a glovebox and used as received. Stock solutions of APTMS and TEOS were prepared by suspending in methanol (99.8%; Fisher Scientific) for stock concentrations of 0.114 and 0.089 mM, respectively. Stock solutions of APTMS and TEOS were used to prepare the scaffolded LHNTs.

Ensemble characterization. Ultraviolet–visible absorption spectroscopy (Agilent; Cary) and fluorescence spectroscopy (Horiba Jobin Yvon) were used to monitor changes to the supramolecular structure of unscaffolded and scaffolded LHNTs. The surface conductivity was measured using a Zetasizer Nano ZS (Malvern Panalytical).

Cryo-TEM. High-resolution characterization of samples was performed with cryo-TEM. Within 1 h of preparation, 4.5 µl of scaffolded LHNTs was deposited on glow-discharged lacey carbon grids with ultrathin carbon film (Ted Pella; 01895-F) and vitrified in liquid ethane using a freeze-plunging device (Vitrobot; FEI), then imaged at liquid nitrogen temperatures using Halo TEM (FEI) or Tecnai Spirit TEM (FEI) operating at 300 kV with a 2 k × 2 k Gatan wide-angle charge-coupled device (CCD) detector or at 120 kV with a 4 k × 4 k Eagle CCD detector (pixel size = 2.4 Å) with ~2–3 µm defocus to optimize phase contrast.

Heat stress of LHNTs. Samples were heat stressed in a portable thermocycler (Cole-Parmer). Within 1 h of preparation, a 125 µl sample was heated to 100 °C at a ramp rate of 0.3 °C min^{-1}, then brought to room temperature at the same rate, with a final hold temperature of 23 °C. Changes to the supramolecular structure were monitored in situ with ultraviolet–visible absorption spectroscopy during heating and annealing cycles.

NSOM. Samples of unscaffolded and scaffolded LHNTs were immobilized onto glass substrates via the drop-flow method[36]. Collection of near-field emission was performed with a multifunctional near-field scanning optical microscope equipped with a piezo-driven scan stage (WITec; alpha300 RS). A continuous-wave laser (Coherent; Compass Sapphire; excitation = 488 nm; output = 72 mW) was coupled to a single-mode optical fibre (WITec; 187643) and passed through an excitation objective (Zeiss; EC Epiplan 20×/0.4; free working distance (FWD) = 3.2 mm) to focus through an aperture of NSOM cantilevers (WITec; drive amplitude = 0.3 V; resonance frequency = 178 kHz). The sample was raster scanned in the x and y directions by a piezo-driven scan stage and the emission was collected through a detection objective (Nikon CFI Achro; 60×/0.8; FWD = 3.0 mm), filtered through 532 nm long-pass filter (Semrock; BLP01-532R-25), then fibre-coupled to an ultra-high-throughput spectrometer (WITec; UHTS 300; G1 = 600 g mm^{-1}; centre wavelength = 560 nm) equipped with an electron-multiplying CCD camera (Andor; Newton 970; 1,600 × 200 array; 16 µm × 16 µm pixel size). The force threshold between the tip and sample was stabilized at 0.27 V, with 2% proportional and 4% integral gains.

Broadband femtosecond transient absorption spectroscopy. The experimental apparatus[49] consisted of a Ti:sapphire oscillator (80 MHz; 790 nm; 30 nm full width at half maximum; 8 nJ) that seeded a Ti:sapphire amplifier to yield laser pulses at a 1.25-kHz repetition rate (11 nm full width at half maximum; 700 µJ; 0.1% shot-to-shot relative standard deviation). Each pulse seeded a custom-built noncolinear optical parametric amplifier that resulted in broadband laser pulses of 500–760 nm at 200 nJ, with 0.5 shot-to-shot relative standard deviation. The pulse duration of the noncolinear optical parametric amplifier output was subsequently compressed to 6.5 fs, as measured by transient-grating frequency-resolved optical gating using a prism-based pulsed shaper utilizing an adaptive neural network algorithm[50]. The compressed laser pulse was split into a boxcar geometry where two beams constituted the pump and probe arms. The pump pulse was modulated by a delay stage and the probe pulse was attenuated with a neutral density filter to be 10^4 less intense than the pump. Transient absorption measurements were performed using between 12 and 15 µW of the pump power at 1,600 kinetic cycle pairs. Little change in the transient absorption profile was observed between pump powers of 460 and 40 µW.

DSSC fabrication and characterization. The cells were prepared with working electrodes with a manually measured 0.25 cm^2 area of nanoporous zinc oxide film applied to fluorine-doped SnO_2 conductive glass. All films were sintered at 400 °C for 30 min and sensitized with dye at room temperature. Counter electrodes were prepared by vapour-phase deposition of ~7 nm platinum to fluorine-doped SnO_2 glass. Electrolyte solutions consisted of 0.5 M iodine and 0.5 M lithium iodide dissolved in acetonitrile. The cells were prepared under ambient conditions and fabricated by applying pressure to seal the working electrode and counter electrode together with double-sided adhesive spacer. Cells were illuminated under white light (0.29 mW cm^{-2}) during linear sweep measurements (Gamry Potentiostat) operating at scan rate of 10 mV s^{-1} with a step size of 1 mV.

SEM. Samples of heat-stressed scaffolded LHNTs were prepared for SEM imaging by first depositing aliquots (8 µl) of solution on cleaned, 500-µm-thick P-type B-doped silicon wafer chips with a resistivity of 1–10 Ω cm (University Wafer). To facilitate adsorption of the scaffolded LHNT solution onto the surface of the silicon chip, the droplet was allowed to evaporate at room temperature. To improve the sample imaging contrast, a 2.5-nm layer of gold was sputtered over the sample-adsorbed silicon substrate using a Leica EMACE200 Coater. SEM images were captured using an FEI Helios NanoLab 660 focused-ion-beam scanning electron microscope and secondary-electron detector (Everhart–Thornley).

Data availability

The data that support the findings of this study are available from the corresponding author upon reasonable request. Source data are provided with this paper.

References

47. Lyon, J. L. et al. Spectroelectrochemical investigation of double-walled tubular J-aggregates of amphiphilic cyanine dyes. *J. Phys. Chem. C* **112**, 1260–1268 (2008).
48. Qiao, Y., Polzer, F., Kirmse, H., Kirstein, S. & Rabe, J. P. Nanohybrids from nanotubular J-aggregates and transparent silica nanoshells. *Chem. Commun.* **51**, 11980–11982 (2015).
49. Bizimana, L. A., Brazard, J., Carbery, W. P., Gellen, T. & Turner, D. B. Resolving molecular vibronic structure using high-sensitivity two-dimensional electronic spectroscopy. *J. Chem. Phys.* **143**, 164203 (2015).
50. Farfan, C. A., Epstein, J. & Turner, D. B. Femtosecond pulse compression using a neural-network algorithm. *Opt. Lett.* **43**, 5166–5169 (2018).

Acknowledgements

This material is based on work partially supported by the National Science Foundation (NSF) Faculty Early Career Development Program (NSF-CAREER 1752475) and US Department of Energy, Office of Science, Office of Basic Energy Sciences. Equipment support was partially provided by the NSF Major Research Instrumentation Program (NSF-MRI 1531859). Financial support for the time-resolved spectroscopic studies was partially provided by the US Department of Energy, Office of Science, Office of Basic Energy Sciences (DE-SC0018142). Support for the solar cell design and fabrication was partially provided by the NSF-CREST Center for Interface Design and Engineered Assembly of Low Dimensional Systems (IDEALS) (NSF grant HRD-1547830). D.M.E., N.V. and P.G. acknowledge partial support from the US Department of Energy, Office of Science, Office of Basic Energy Sciences (DE-SC0018142). M.W. acknowledges support from the NSF-CREST IDEALS Fellowship. W.P.C. acknowledges partial support from the Margaret Strauss Kramer Fellowship. S.J.J. is supported by the NSF (CHE-1900170) and the US Department of Energy, Office of Sciences, Office of Basic Energy Sciences (DE-SC0001393). This work was performed in part at the Center for Discovery and Innovation (CDI) of The City College of New York and the Advanced Science Research Center (ASRC) Imaging Facility of The City University of New York. We thank the Martin and Michele Cohen Fund for Science, the PSC-CUNY Research Award Program, WITec GmbH, Tavid Ezell, David M. Milch and Tony Liss for generous support.

Author contributions

D.M.E. directed the project. K.N. synthesized the samples, performed the ensemble, cryo-TEM and NSOM measurements and temperature-dependent studies, analysed the experimental data, initiated collaboration with M.W. and I.K. and prepared the samples for linear sweep voltammetry measurements. N.V. and P.G. prepared samples for the time-resolved spectroscopy experiments, N.V. performed the SEM measurements, and W.P.C. and K.N. performed the time-resolved spectroscopy measurements and analysed the experimental data. K.N. and M.W. designed and fabricated the DSSCs under the guidance of I.K. and K.N. analysed the experimental data under the guidance of D.M.E. S.J.J. contributed to the interpretation of spectroscopic data of heat-stressed samples. All authors provided fruitful discussions and beneficial interpretation of the data and analyses. K.N. and D.M.E. co-wrote the manuscript with input from all authors.

Competing interests

The authors declare no competing interests.

Additional information

Supplementary information is available for this paper at https://doi.org/10.1038/s41557-020-00563-4.

Correspondence and requests for materials should be addressed to D.M.E.
Reprints and permissions information is available at www.nature.com/reprints.